doi:10.1016/j.jmb.2003.08.032 J. Mol. Biol. (2003) 333, 367–376

JMB

Available online at www.sciencedirect.com

SCIENCE DIRECT®

ELSEVIER

# Crystal Structures of the Free and Anisic Acid Bound Triple Mutant of Phospholipase $A_2$

**K. Sekar[1,2]*, S. Vaijayanthi Mala[3], M. Yogavel[3], D. Velmurugan[3] Ming-Jye Poi[4], B. S. Vishwanath[5], T. V. Gowda[5] A. Arokia Jeyaprakash[6] and M.-D. Tsai[4]**

[1]*Bioinformatics Centre, Indian Institute of Science, Bangalore 560 012, India*

[2]*Supercomputer Education and Research Centre, Indian Institute of Science, Bangalore 560 012, India*

[3]*Department of Crystallography and Biophysics University of Madras, Guindy Campus, Chennai 600 025 India*

[4]*Departments of Chemistry and Biochemistry and the Ohio State Biochemistry Program The Ohio State University Columbus, OH 43210, USA*

[5]*Department of Studies in Biochemistry, University of Mysore, Masasagangothri Mysore 570 006, India*

[6]*Molecular Biophysics Unit Indian Institute of Science Bangalore 560 012, India*

**Corresponding author*

Phospholipase $A_2$ catalyses the hydrolysis of the ester bond of 3-*sn*-phosphoglycerides. Here, we report the crystal structures of the free and anisic acid-bound triple mutant (K53,56,120M) of bovine pancreatic phospholipase $A_2$. In the bound triple mutant structure, the small organic molecule *p*-anisic acid is found in the active site, and one of the carboxylate oxygen atoms is coordinated to the functionally important primary calcium ion. The other carboxylate oxygen atom is hydrogen bonded to the phenolic hydroxyl group of Tyr69. In addition, the bound anisic acid molecule replaces one of the functionally important water molecules in the active site. The residues 60–70, which are in a loop (surface loop), are disordered in most of the bovine pancreatic phospholipase $A_2$ structures. It is interesting to note that these residues are ordered in the bound triple mutant structure but are disordered in the free triple mutant structure. The organic crystallization ingredient 2-methyl-2,4-pentanediol is found near the active site of the free triple mutant structure. The overall tertiary folding and stereochemical parameters for the final models of the free and anisic acid-bound triple mutant are virtually identical.



*Keywords:* anisic acid; triple mutant; phospholipase $A_2$; crystal structure; surface loop

## Introduction

Phospholipase $A_2$ (PLA2; EC 3.1.1.4) is an extracellular, calcium-dependent lipolytic enzyme that cleaves specifically the *sn*-2 fatty acid ester bond of L-glycerophospholipid. Arachidonic acid is the precursor of the eicosanoid mediators of several inflammations, for example thromboxanes and prostaglandins, and blood platelet aggregation. Several PLA2s have been extracted from mammalian pancreas, which require calcium ion for their enzymatic activity. In view of this pharmacological interest, considerable attention has been paid to selecting potential inhibitors of the enzyme and designing a suitable drug. To this end, several crystal structures of tetrahedral mimic inhibitors complexed with PLA2 from different families are available.[1–6] These studies have generated immense pharmacological interest and shed light on the mechanism of action of PLA2. In addition, other inhibitors (without the tetrahedral mimics of phospholipids) are available (but fewer) in the

Abbreviations used: MPD, 2-methyl-2,4-pentanediol; PLA2, phospholipase $A_2$; rmsd, root-mean-square deviation; WT, wild-type.

E-mail address of the corresponding author: sekar@physics.iisc.ernet.in

literature.[7–11] Recent biochemical studies indicated the binding of anisic acid (*p*-methoxy benzoic acid) to the basic PLA2 from *Vipera russelli* venom.[12] To gain further understanding and unravel the mode of binding of anisic acid, we have co-crystallized anisic acid with the triple mutant (K53,56,120M) of bovine pancreatic PLA2. The reason for studying this triple mutant is as follows.

The interfacial-binding site is a unique feature and one of the important structural features for the catalytic reaction of PLA2.[13–16] The importance and involvement of the interfacial binding residues in interfacial catalysis have been outlined.[17–21] Yu *et al*.[22] have suggested a concurrent role for several cationic residues, possibly Lys53, Lys56, Lys120 and Lys121, in determining the anionic interface preference of these diverse types of secreted PLA2. They have shown that the lysine-to-methionine substitution of residues 53, 56, 120 and 121 eliminates the anionic interface preference of the wild-type (WT) and enhances its preference for the zwitterionic interface. Recently, the crystal structure of triple mutant (K56,120,121M) reported from our laboratory (involving three of the four cationic residues) revealed the position of the secondary calcium ion for the first time in the history of bovine pancreatic PLA2.[23] In view of the above, we have undertaken the crystal structures of the free and complex forms of the triple mutant (K53,56,120M) of bovine pancreatic PLA2. The structural details and results are discussed below.

**Table 1.** Crystal and other pertinent geometrical parameters of the free and bound triple mutant (K53, 56,120M) of bovine pancreatic PLA2

| | Free triple mutant | Triple mutant + anisic acid |
|---|---|---|
| *Unit cell parameters* | | |
| *a* (Å) | 46.76 | 46.61 |
| *b* (Å) | 46.76 | 46.61 |
| *c* (Å) | 102.71 | 102.68 |
| Space group | $P3_121$ | $P3_121$ |
| Resolution range (Å) | 19.9–1.85 | 19.8–2.6 |
| No. observations | 76,651 | 22,211 |
| Unique reflections | 11,084 | 3957 |
| $R_{merge}$ (%) | 6.0 | 15.1 |
| Cumulative completeness (%) | 95.0 | 92.2 |
| $R_{work}$ (%) | 19.3 | 18.7 |
| $R_{free}$ (%) | 23.2 | 24.1 |
| *Protein model* | | |
| Protein atoms | 954 | 954 |
| Bound calcium ion | 1 | 1 |
| Water molecules | 85 | 43 |
| MPD/inhibitor atoms | 8 | 11 |
| *RMS deviations from* | | |
| Ideal bond lengths (Å) | 0.005 | 0.006 |
| Ideal bond angles (deg.) | 1.2 | 1.2 |
| Ideal dihedral (deg.) | 22.2 | 22.0 |
| Ideal improper (deg.) | 0.70 | 0.72 |
| *Average temperature factors* (Å$^2$) | | |
| Main-chain atoms | 27.9 | 23.6 |
| Side-chain atoms | 31.4 | 28.3 |
| Water molecules | 39.2 | 33.3 |
| Calcium ion ($Ca^{2+}$) | 23.0 | 21.1 |
| MPD/inhibitor atoms | 45.8 | 37.1 |

$R_{merge} = \sum_{hkl}|I - \langle I\rangle|/\sum I$, where $I$ is the observed intensity and $\langle I\rangle$ is the average intensity from observations of symmetry-related reflections, respectively.

## Results and Discussion

### Free triple mutant structure

A very clear electron density was observed for all the regions in the protein model, except the surface loop (residues 60–70). This region is generally disordered in most of the bovine recombinant PLA2 structures reported in the literature. Table 1 gives the root-mean-square deviations (rmsd) from the ideal geometry for the bond lengths, bond angles and dihedral angles. From the σ(A) method, the coordinate error is estimated to be 0.18 Å. The program PROCHECK was used to assess the quality of the final model.[24] A total of 93.6% of the residues are found in the most favored regions of the Ramachandran plot and the remaining residues are in the additionally allowed region.[25] None of the residues is in the disallowed region. The relevant refinement and stereochemical parameters are given in Table 1. A ribbon diagram of the structure of the free triple mutant is shown in Figure 1.

The backbone atoms of the free triple mutant structure show an rmsd of 0.36 Å with the trigonal WT enzyme, the starting model.[26] This suggests that the overall folding of the free triple mutant structure is very similar to that of the WT enzyme. As found in the trigonal and orthorhombic WT enzymes of PLA2, the active-site cleft consists of the commonly found five water molecules (see the discussion below for details) including the conserved structural water molecule. In addition, a 2-methyl-2,4-pentanediol (MPD) molecule from the organic solvent used in crystallization binds near the active site (Figure 2). The catalytically important primary calcium ion has seven ligands, which exhibit pentagonal bipyramidal coordination.

### Triple mutant with anisic acid bound

The quality of the protein model was very good as assessed by the program PROCHECK.[24] The Ramachandran plot[25] showed that all (ϕ,φ) angles are in the most favored and additionally allowed regions, with none of the residues in the disallowed region of the plot. The σ(A) method indicated an estimated error of 0.12 Å in the atomic coordinates. A summary of the refined model and the relevant geometrical parameters are given in Table 1. The electron density is very clear for almost all the regions of the model. In contrast to the observation from the free triple mutant structure, it is interesting to note that the electron density is very clear for all the residues in the surface loop (residues 60–70) (Figure 3). Here, the

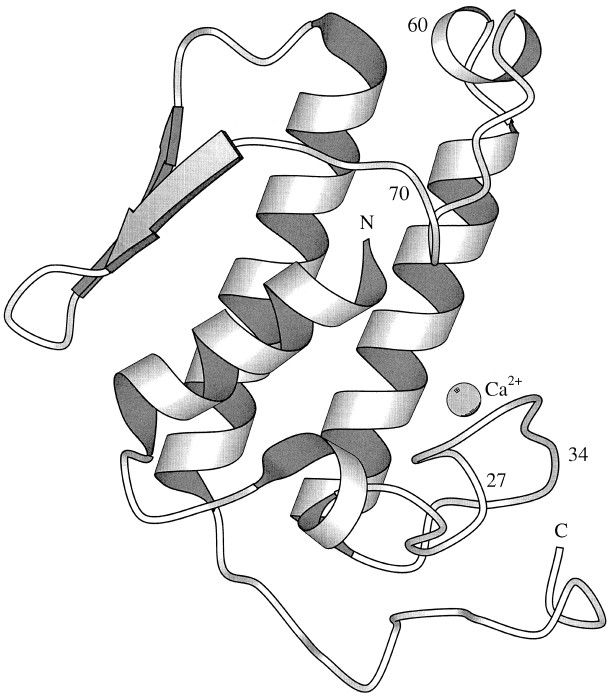


**Figure 1**. The backbone tracing of the free triple mutant. The surface loop residues (60–70) and the calcium-binding loop (27–34) are indicated with the residue numbers at the beginning as well as at the ends. This Figure was produced using the program MOLSCRIPT.[44]

active site is occupied by the anisic acid molecule and the electron density is shown in Figure 4. Three of the five commonly found water molecules are found to be missing (see below for details). The backbone α-carbon atoms of the bound triple mutant structure superpose well with the trigonal WT enzyme, with an rmsd of 0.28 Å. Large deviations are seen in the surface loop residues.

The α-carbon atoms of the free and bound triple mutant structures reported here superpose very well, with an rmsd of 0.32 Å, indicating that the overall tertiary fold is almost identical. On the other hand, there are several significant differences between the free and the anisic acid-bound structures, which are addressed in detail in the following sections.

## Five active-site water molecules

Five water molecules are generally found in the active site of bovine pancreatic PLA2 structures and are believed to be intimately involved in the enzymatic function of PLA2. These five water molecules were observed in the free triple mutant as described here. Out of the five water molecules, two water molecules are involved in providing coordination (axial, W12, and equatorial, W5) to the functionally important primary calcium ion (Figure 2). The other two water molecules (catalytic water (W6) and second water (W7)) are hydrogen bonded to the imidazole nitrogen atom of His48. These water molecules lie on either side of the imidazole ring of His48. The histidine water molecules

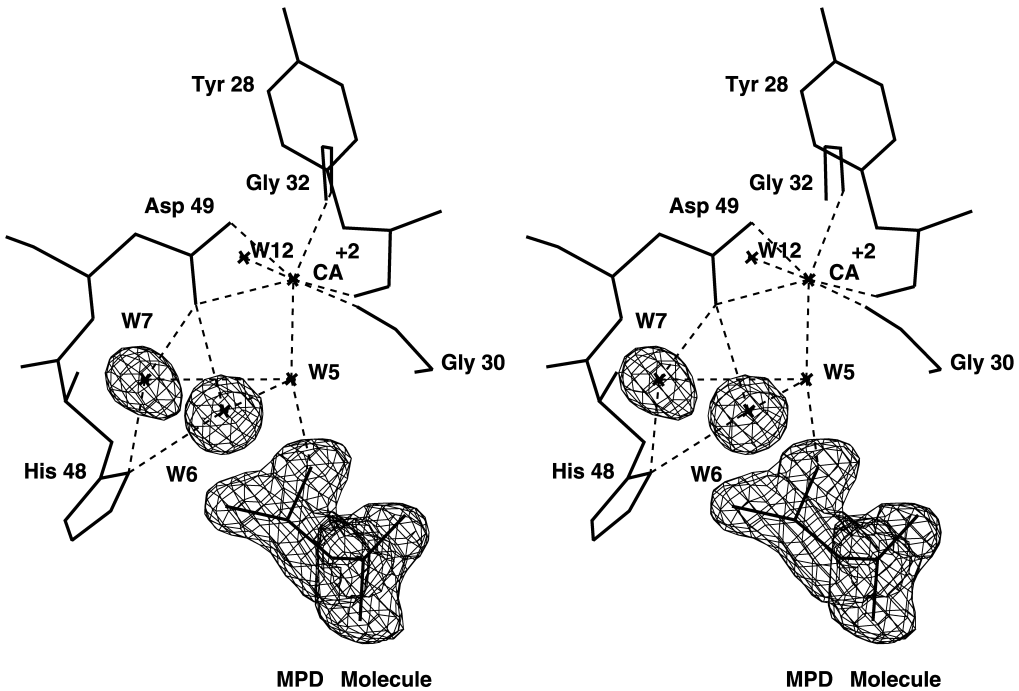


**Figure 2**. The difference electron density map showing the presence of the MPD molecule in the active site of the free triple mutant structure. In addition, the electron density is shown for the two histidine water molecules, catalytic water (W6) and second water (W7). The water molecule W6 is 0.9 Å above the His48 imidazole plane, whereas W7 is 1.76 Å below the plane.

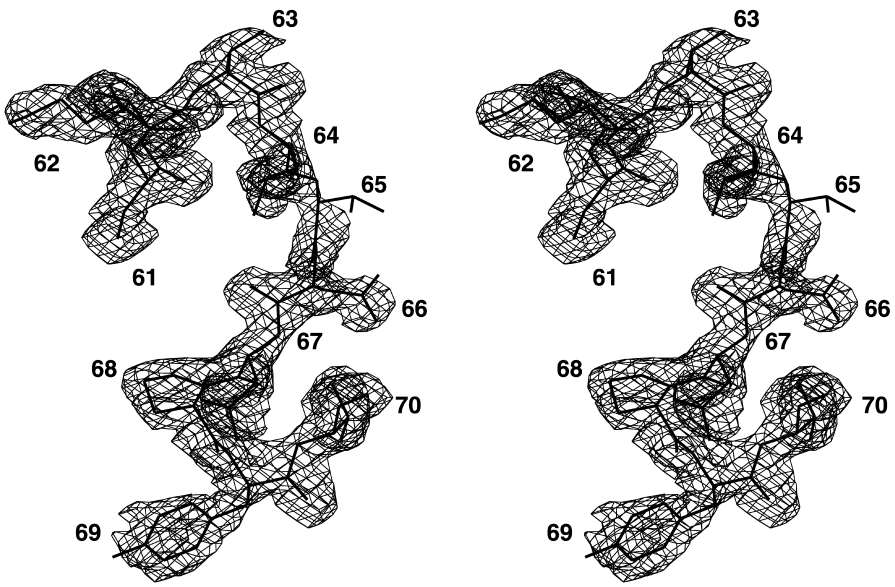


**Figure 3**. A stereo view of the electron density ($2|F_o| - |F_c|$) map showing the ordered surface loop residues 60–70 in the bound triple mutant structure. The electron density is generally very clear, except for the side-chain atoms of the residue Val65.

subtend an angle of 69° at $N^{\delta 1}$.[27] Earlier, we proposed that the second water molecule could be assisting the catalytic water molecule in the tautomerization of His48 for enzyme hydrolysis. The remaining water molecule, designated the conserved structural water molecule, is found in almost all PLA2 structures studied so far. This water molecule forms a network of hydrogen bonding to the surrounding residues (Ala1, Asp99, Tyr52, Tyr73 and Pro68) and has been proposed to serve as a link between the active site and the interfacial recognition site.[28,29]

The inhibitor oxygen atoms generally replace three (two calcium-coordinated water molecules and catalytic water) of the five important water molecules.[1–6] Surprisingly, in one of the PLA2-inhibitor complex structures,[7] only the equatorial calcium-coordinated water molecule is replaced by the oxygen atoms of the inhibitor *n*-dodecyl phosphorylcholine. In the structure of the triple

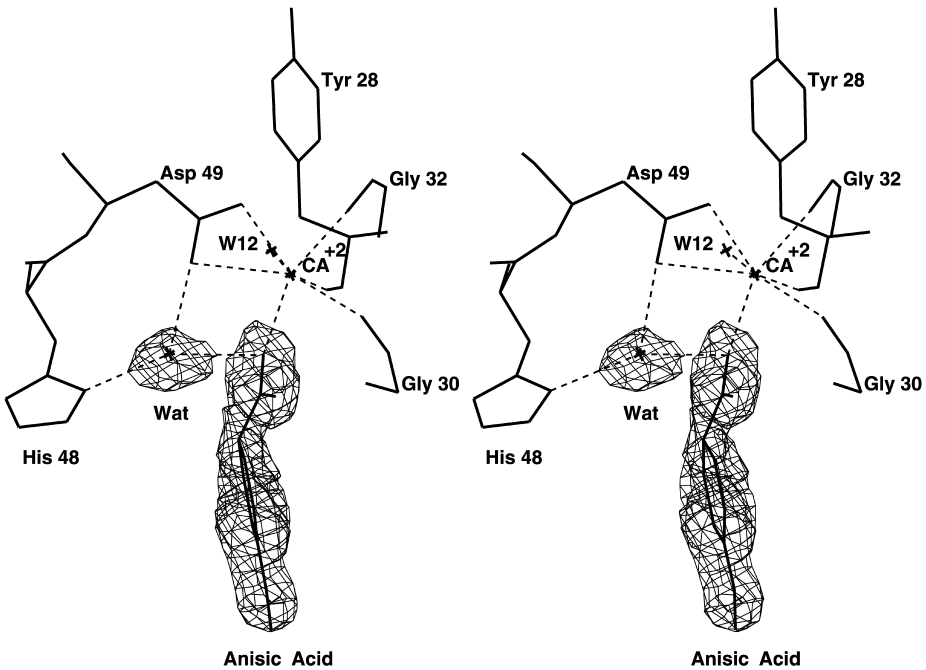


**Figure 4**. Stereo view of the omit electron density map contoured at the 1.0σ level showing the electron density for the anisic acid molecule in the bound triple mutant structure. In addition, the only water molecule hydrogen bonded to $N^{\delta 1}$ of His48 is shown and it is 0.49 Å below the plane of the histidine ring.

mutant with anisic acid bound, there are significant perturbations in the five active-site water molecules, as addressed in the following two sections.

### Anisic acid binds to the active site

Anisic acid is a simple organic molecule and its chemical nature is completely different from the inhibitors (specifically designed for PLA2) available in the literature. In the anisic acid-bound triple mutant structure, the electron density is exceptionally clear for all the atoms of anisic acid molecule (Figure 4), allowing an informative description of the interactions of the inhibitor molecule with the surrounding protein atoms. The carboxylate oxygen atoms of the bound anisic acid are located between the catalytically important calcium ion and the surface loop. The methoxy group of the anisic acid molecule is located on the other side of the primary calcium ion and is involved in interactions with the residues in the entrance of the active site. In the anisic acid-bound structure, one of the carboxylate oxygen atoms replaces the equatorial water molecule (W5) coordinated to the calcium ion with hardly any structural perturbation in the calcium coordination geometry (Figure 4). The other carboxylate oxygen atom of the inhibitor molecule is hydrogen bonded to the phenolic hydroxyl oxygen atom of the residue Tyr69, from the surface loop. Earlier crystallographic investigations revealed that the equatorial calcium-coordinated water molecule is involved in enzyme hydrolysis.[1–3,30] A similar mode of binding was observed earlier in the R-2-dodecanoylamino-1-hexaanolphosphoglycol-PLA2 complex[6] and in the *n*-dodecylphosphorylcholine complex.[7] It is interesting to note that the above two inhibitors are tetrahedral mimics of phospholipids. In contrast to the earlier observations, the axial coordinated water molecule is retained. The calcium–ligand distances vary between 2.24 Å and 2.70 Å, with an average of 2.43 Å, the longest being that of the first ligand (2.70 Å) of Asp49. The average temperature factor for the anisic acid molecule is 37.1 $Å^2$. Upon binding, the catalytic water molecule was removed (Figure 4) and the second water molecule had moved down (on the plane of the imidazole ring of His48) to provide a link between the oxygen atom of the anisic acid and $N^{\delta 1}$ of His48.

### Conserved structural water molecule

The conserved structural water hydrogen bonded to Ala1, stabilizing the interfacial recognition site residues (Ala1, Pro68, Tyr52, Asp99 and Tyr73), is missing (Figure 5(a)) when compared to the earlier PLA2-inhibitor complexes,[2,4] whereas it is present in the free triple mutant structure (Figure 5(b)). Previously, we have shown that the conserved structural water molecule is missing from the single mutant D99N,[31] and from the triple mutant Y52,73F/D99N.[32] However, these crystal structures clearly show the movement of the residue Ala1 towards the void created by the conserved structural water molecule. In contrast to the above observation, there is no movement of the residue Ala1 (Figure 6) in our present complex structure though the conserved structural water molecule is missing. The earlier studies on the single mutant D99N[31] and triple mutant Y52,73F/D99N[32] clearly demonstrated that the active-site Asp99 is essential to preserve the conserved structural water molecule, which in turn stabilizes the interfacial recognition site residues. All atoms of the residues Ala1, Pro68, Tyr52, Tyr73, Asp99 and His48 of free and anisic acid-bound triple mutant structures superpose well (rmsd 0.18 Å). Lack of the conserved structural water molecule does not mean that it is actually not there. It could be there but is more mobile and not detectable. By keeping the above points in mind, we conclude that the conserved structural water molecule missing from the anisic acid-bound triple mutant structure could be due to the crystallographic artifact.

### Ordered surface loop

In most of the bovine pancreatic PLA2 and its mutant structures studied so far,[5,22,27,33,34] the surface loop residues were always found to be disordered, except in the high-resolution (1.5 Å) orthorhombic form[26] of the recombinant PLA2. Again in the present free triple mutant structure, the electron density is not clear and the surface loop residues are disordered. In contrast, the electron density for the surface loop in the bound triple mutant structure is very clear and ordered (Figure 3), except for the end atoms of the residue Val65. A possible interpretation for this observation is that the surface loop in the bound triple mutant structure participates in binding to the anisic acid molecule and this, in turn, helped in the ordering of the surface loop residues. As pointed out above, the phenolic hydroxyl group of Tyr69 hydrogen bonds with one of the carboxylate oxygen atoms of the anisic acid molecule and helps to anchor the inhibitor molecule in the active-site cleft.[35] Further studies are required to understand the structural and functional basis of the loop dynamics.

Binding of the MPD molecule from the organic solvent used in crystallization to the "free" PLA2 was observed previously and is observed again in the free triple mutant reported here. In the bound triple mutant structure, the anisic acid molecule occupies the active site (Figure 4), whereas the MPD molecule in the free triple mutant structure binds differently (Figure 2). One of the hydroxyl groups of the MPD molecule is hydrogen bonded to a water molecule, which is a natural ligand, to the catalytically important calcium ion. The other hydroxyl oxygen atom is involved in hydrogen bonding with the main-chain carbonyl group of Phe22 (which is in the entrance of the active site) and the amide nitrogen atom of Gly30. The

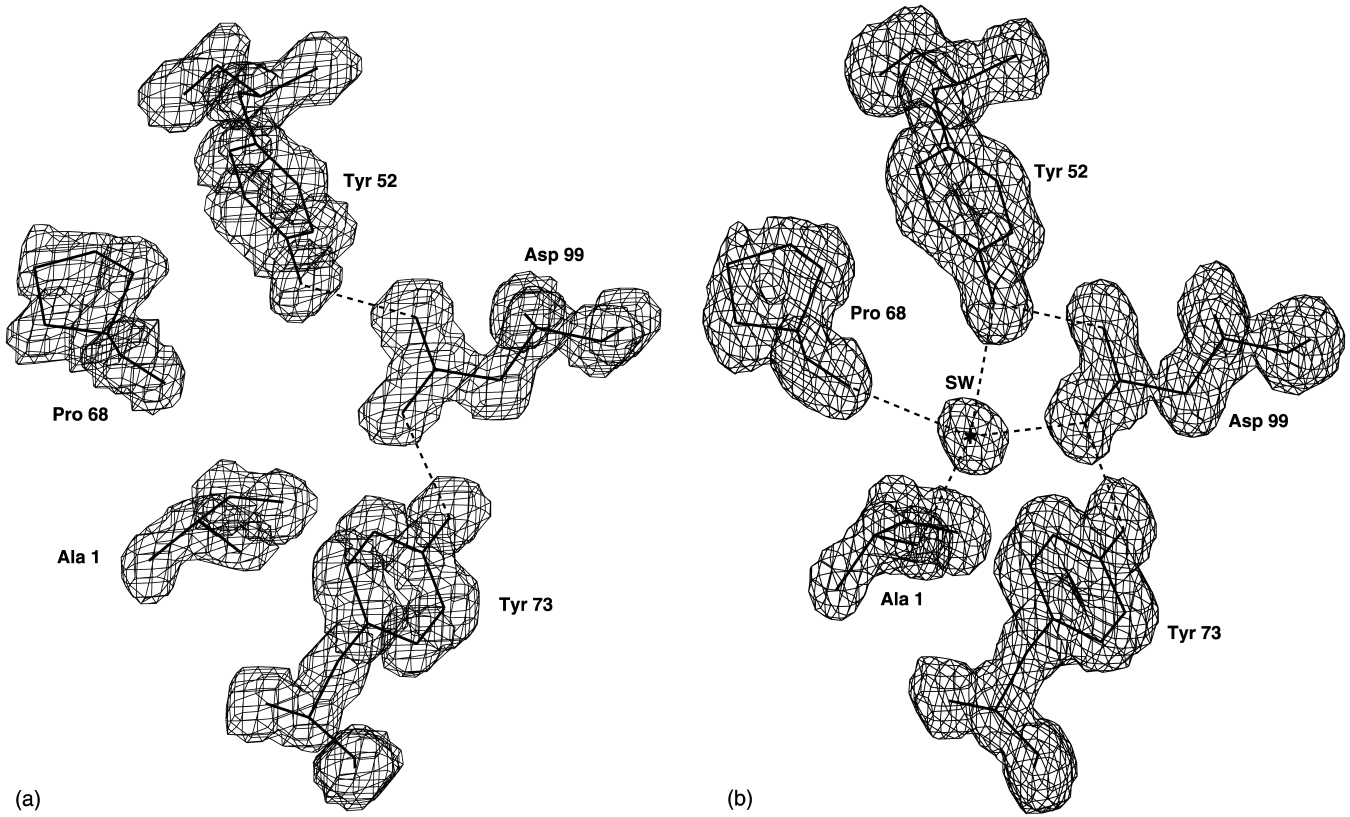


**Figure 5**. The electron density contoured at the 1.0σ level showing the interfacial recognition site residues and their hydrogen bonding network in (a) the anisic acid-bound and (b) free triple mutant structures. The only difference is that the electron density for the conserved structural water (SW) is missing from the anisic acid-bound triple mutant structure.

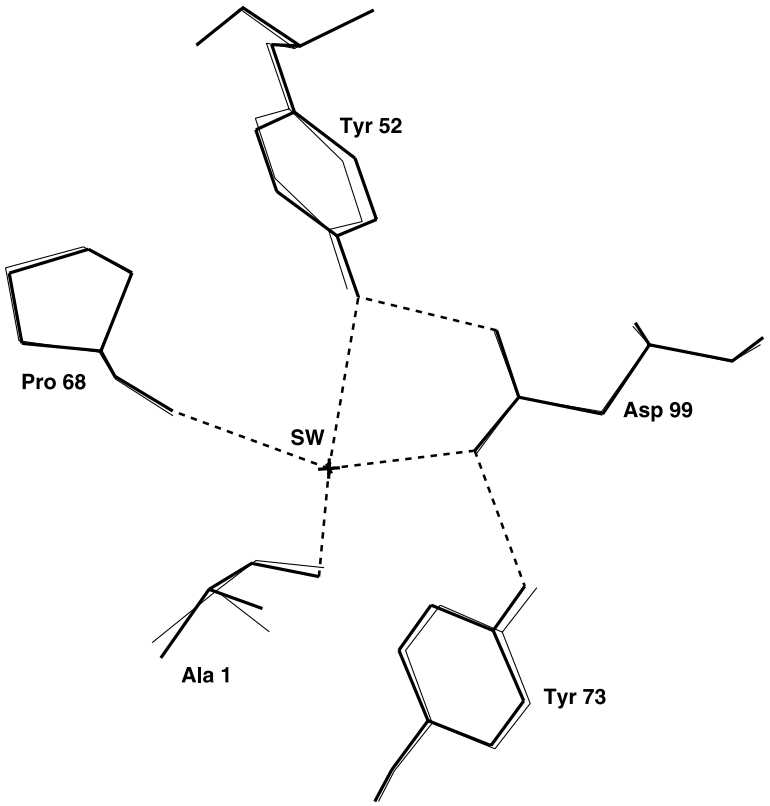


**Figure 6**. Superposition of the residues around the conserved structural water in the free (thick lines) and anisic acid-bound (thin lines) triple mutant structures. It is clear that the water molecule SW is missing from the bound triple mutant structure without any structural perturbation.

interactions of the oxygen atoms of the MPD molecule in the free triple mutant structure are different compared to the earlier reports.[36]

## Conclusions

The three-dimensional crystal structures of the free and the bound triple mutant (K53,56,120M) of the recombinant PLA2 have been determined at 1.85 Å and 2.6 Å resolution, respectively. The overall fold of the two reported structures is similar to that of the trigonal form of the WT PLA2 structure. An interesting observation is that the surface loop residues are ordered in the anisic acid-bound structure, while this loop is disordered in the free triple mutant structure. In the bound structure, the anisic acid molecule replaces the equatorial water molecule involved in the calcium coordination. Also, only one water molecule is hydrogen bonded to His48 and is on the plane of the imidazole ring. It is noteworthy that the conserved structural water molecule is missing from the structure of the complex, whereas it is present in the free triple mutant structure. Whether it is caused by a crystallographic artifact in the former case remains to be determined. Three out of the five functionally important water molecules are found to be missing. Though the organic molecule, anisic acid, does not resemble the true tetrahedral mimicking phospholipids, the present study opens a new avenue for knowledge-based rational drug design using simple organic molecules.

## Materials and Methods

### Construction of the K53,56,120M PLA2 mutant

The mutant PLA2 was generated by site-directed mutagenesis. The following complementary sets of oligonucleotides were used:

5′ CATGATAATTGCTA TATGCAAGCTAAAAA ACTT 3′ (K53 to M)
5′ TGCTATAAACAAGCTA TGAAACTTGATAG CTGC 3′ (K56M)
5′ CACAAGAATCTTGATATGAA AAACTGTTAA GCTT 3′ (K120M)

The Quickchange™ method by Stratagene was employed using pET25b(m)-pro$PLA_2$ as template. First, the single mutant K53M was generated, then the double (K53/56M) and triple (K53/56/120M) mutants were generated using the single mutant and double mutant, respectively, as template DNA. The recombinant $PLA_2$ protein was expressed in *Eschericha coli* BL21 (DE3) pLysS strain (Novagen) as inclusion bodies, which was refolded and purified as described.[17,37]

### Crystallization, data collection, structure solution and refinement of the free triple mutant K53,56,120M

Crystals of the triple mutant were obtained using the hanging-drop, vapor-diffusion method at room temperature (293 K). The crystallization conditions were similar to those described earlier.[26] The intensity data were collected using the area detector system powered by a Rigaku generator at 44 kV and 70 mA. The atomic coordinates of the trigonal form of recombinant PLA2[26] (PDB-id code 1MKT) were used as the starting model

for the refinement. A total of 896 reflections were used to calculate the free *R*-value[38] to check the progress of refinement. A few cycles of the rigid body refinement followed by 100 steps of Powell energy minimization on the positions were carried out. The crystallographic *R*-value dropped to 25.6% ($R_{free} = 27.1\%$) without the mutated residues for all reflections in the resolution range 19.87–1.85 Å. The three residues Lys53, Lys56 and Lys120 were mutated to methionine using the difference electron density maps calculated at this stage. The model was then subjected to simulated annealing using residual function mlf as implemented in the refinement package CNS (version 1.1).[39] The functionally important calcium ion and the MPD molecule were located. In all, 85 water oxygen atoms were located and included in the refinement during the progress of refinement. The final *R*-value was 19.3% ($R_{free} = 23.2\%$). The final refined model consists of 954 non-hydrogen protein atoms, one calcium ion, 85 water molecules and one MPD molecule. The necessary crystal data and relevant refinement parameters are given in Table 1.

### Crystallization, data collection, structure and refinement of PLA2 + anisic acid bound model

Crystals of the triple mutant PLA2-anisic acid complex were obtained by co-crystallization, which was carried out by the hanging-drop, vapor-diffusion method at room temperature (293 K). The crystallization droplet contained 5 μl of the protein at a concentration of 17–20 mg $ml^{-1}$, in 50 mM Tris–HCl (pH 7.2), 5 mM $CaCl_2$, 3 μl of 60% (v/v) MPD and 1 μl of anisic acid solution (higher molar concentration) against the reservoir concentration of 70% MPD. The crystals were trigonal ($P3_121$) with unit cell parameters $a = b = 46.61$ Å and $c = 102.68$ Å (one molecule in the asymmetric unit). X-ray diffraction data were collected from a single crystal measuring 0.20 mm × 0.30 mm × 0.40 mm on our in-house area detector at room temperature (293 K). The data were integrated, scaled and reduced to 2.6 Å resolution with DENZO[40] and SCALEPACK.[41] A total of 22,211 observations were recorded, which gave 3957 unique reflections to 2.6 Å resolution. The three-dimensional atomic coordinates of the trigonal form[26] (PDB-id code 1MKT) solved at 1.72 Å were used as the starting model to refine the present anisic acid-bound PLA2 model, since the molecular orientation and position of this model in the unit cell were almost isomorphous with those in the free triple mutant reported here. Out of 3957 unique reflections, a total of 240 reflections were kept separately for the calculation of $R_{free}$, to monitor the progress of the refinement.[38] Twenty-five cycles of rigid body refinement gave an *R*-value of 30.9% ($R_{free} = 34.5\%$). The difference electron density maps calculated at this stage were used to locate the catalytically important calcium ion and the three mutated residues. In addition, the difference maps clearly revealed the electron density for all the atoms of the anisic acid molecule. During the progress of the refinement, 43 water oxygen atoms were picked and included in the refinement. Simulated annealing omit maps were calculated (omitting 15 residues at a time) (as implemented in the refinement program CNS(1.1)) and were used to correct the protein model. The final protein-anisic acid complex model contains 954 protein atoms (from 123 residues), one $Ca^{2+}$, 43 water oxygen atoms and one anisic acid molecule. Refinement of the model including the water molecules gave a final *R*-value of 18.7% ($R_{free} = 24.1\%$) for all reflections (without any sigma cut-off) in the resolution range 19.98–2.6 Å. The molecular graphics and modeling program FRODO[42] was used throughout the model building followed by the program CNS(1.1) for refinement.

### Data Bank accession numbers

The atomic coordinates and structure factors have been deposited with the Protein Data Bank,[43] Research Collaboratory for Structural Bioinformatics, USA (reference 1O3W for atomic coordinates and reference R1O3WSF for the structure factors).

The atomic coordinates for the triple mutant complex are deposited in the PDB as 1O2E, with R1O2ESF for the structure factors.

## Acknowledgements

The intensity data were collected at the National Data Collection Facility for Structural biology at the Molecular Biophysics Unit, Indian Institute of Science, Bangalore 560 012, India, supported by the Department of Science and Technology (DST) and the Department of Biotechnology (DBT), Government of India. The authors gratefully acknowledge the use of the interactive graphics-based molecular modelling of the Supercomputer Education and Research Centre and the Distributed Information Centre. One of the authors (D.V.) thanks the UGC for financial support. The work from Dr Tsai's laboratory was supported by NIH grants GM 41788 and GM 57568.

## References

1. White, S. P., Scott, D. L., Gelb, M. H. & Sigler, P. B. (1990). Crystal structure of cobra-venom phospholipase $A_2$ in a complex with a transition-state analogue. *Science*, **250**, 1560–1563.
2. Scott, D. L., White, S. P., Otwinowski, Z., Yuan, W., Gelb, M. H. & Sigler, P. B. (1990). Interfacial catalysis: the mechanism of phospholipase $A_2$. *Science*, **250**, 1541–1546.
3. Scott, D. L., White, S. P., Browning, J. L., Rosa, J. J., Gelb, M. H. & Sigler, P. B. (1991). Structures of free and inhibited human secretory phospholipase $A_2$ from inflammatory exudates. *Science*, **254**, 1007–1010.
4. Sekar, K., Eswaramoorthy, S., Jain, M. K. & Sundaralingam, M. (1997). Crystal structure of the complex of bovine pancreatic phospholipase $A_2$ with the inhibitor 1-hexadecyl-3-(trifluoroethyl)-*sn*-glycero-2-phosphomethanol. *Biochemistry*, **36**, 14186–14191.
5. Sekar, K., Kumar, A., Liu, X., Tsai, M.-D., Gelb, M. H. & Sundaralingam, M. (1998). Structure of the complex of bovine pancreatic phospholipase $A_2$ with a transition-state analogue. *Acta Crystallog. sect. D*, **54**, 334–341.
6. Thunnissen, M. M. G. M., Eiso, A. B., Kalk, K. H., Drenth, J., Dijkstra, B. W., Kuipers, O. P. *et al.* (1990). X-ray structure of phospholipase $A_2$ complexed with a substrate-derived inhibitor. *Nature*, **347**, 689–691.
7. Tomoo, K., Ohishi, H., Ishida, T., Inoue, M., Ikeda, K.,

Sumiya, S. & Kitamura, K. (1994). X-ray crystal structure and molecular dynamics simulation of bovine pancreas phospholipase $A_2$-*n*-dodecylphosphorylcholine complex. *Proteins: Struct. Funct. Genet.* **19**, 330–339.
8. Cha, S. S., Lee, D., Adams, J., Kurdyla, J. T., Jones, C. S., Marshall, L. A. *et al.* (1996). High-resolution X-ray crystallography reveals precise binding interactions between human nonpancreatic secreted phospholipase $A_2$ and a highly potent inhibitor (FPL67047XX). *J. Med. Chem.* **39**, 3878–3881.
9. Chandra, V., Jasti, J., Kaur, P., Betzel, Ch., Srinivasan, A. & Singh, T. P. (2002). Structural basis of phospholipase $A_2$ inhibition for the synthesis of prostaglandins by the plant alkaloid aristolochic acid from a 1.7 Å crystal structure. *Biochemistry*, **41**, 10914–10919.
10. Chandra, V., Jasti, J., Kaur, P., Dey, S., Srinivasan, A., Betzel, Ch. & Singh, T. P. (2002). Design of specific peptide inhibitors of phospholipase $A_2$: structure of a complex formed between Russell's viper phospholipase $A_2$ and a designed peptide Leu-Ala-Ile-Tyr-Ser (LAIYS). *Acta Crystallog. sect. D*, **58**, 1813–1819.
11. Chandra, V., Jasti, J., Kaur, P., Betzel, Ch., Srinivasan, A. & Singh, T. P. (2002). First structural evidence of a specific inhibition of phospholipase $A_2$ by alpha-tocopherol (vitamin E) and its implications in inflammation: crystal structure of the complex formed between phospholipase $A_2$ and alpha-tocopherol at 1.8 Å resolution. *J. Mol. Biol.* **320**, 215–222.
12. Uma, B. & Gowda, T. V. (2000). Molecular mechanism of lung hemorrhage induction by VRV-PL-VIIIa from Russell's viper (*Vipera russelli*) venom. *Toxicon*, **38**, 1129–1147.
13. Jain, M. K., Rogers, J., Jahagirdar, D. V., Marecek, J. F. & Ramirez, F. (1986). Kinetics of interfacial catalysis by phospholipase $A_2$ in intravesicle scooting mode, and heterofusion of anionic and zwitterionic vesicles. *Biochim. Biophys. Acta*, **860**, 435–447.
14. Jain, M. K., Rogers, J., Berg, O. G. & Gelb, M. H. (1991). Interfacial catalysis by phospholipase $A_2$: activation by substrate replenishment. *Biochemistry*, **30**, 7340–7348.
15. Dijkstra, B. W., Kalk, K. H., Hol, W. G. J. & Drenth, J. (1981). Structure of bovine pancreatic phospholipase $A_2$ at 1.7 Å resolution. *J. Mol. Biol.* **147**, 97–123.
16. Dijkstra, B. W., Kalk, K. H., Drenth, J., de Haas, G. H., Egmond, M. R. & Slotboom, A. J. (1984). Role of the N-terminus in the interaction of pancreatic phospholipase $A_2$ with aggregated substrates. Properties and crystal structure of transaminated phospholipase $A_2$. *Biochemistry*, **23**, 2759–2766.
17. Noel, J. P., Deng, T., Hamilton, K. J. & Tsai, M.-D. (1990). Phospholipase $A_2$ engineering. 3. Replacement of lysine-56 by neutral residues improves catalytic efficiency significantly, alters substrate specificity, and clarifies the mechanism of interfacial recognition. *J. Am. Chem. Soc.* **112**, 3704–3706.
18. Noel, J. P., Bingman, C., Deng, T., Dupureur, C. M., Hamilton, K. J., Jiang, R. T. *et al.* (1991). Phospholipase $A_2$ engineering. X-ray structural and functional evidence for the interaction of lysine-56 with substrates. *Biochemistry*, **30**, 11801–11811.
19. Maliwal, B. P., Yu, B.-Z., Szmacinksi, H., Squier, T., Binsbergen, J. V., Slotboom, A. J. & Jain, M. K. (1994). Functional significance of the conformational dynamics of the N-terminal segment of secreted phospholipase $A_2$ at the interface. *Biochemistry*, **33**, 4509–4516.
20. Liu, X. H., Zhu, H. X., Huang, B. H., Rodgers, J., Yu, B.-Z., Kumar, A. *et al.* (1995). Phospholipase $A_2$ engineering. Probing the structural and functional roles of N-terminal residues with site-directed mutagenesis, X-ray, and NMR. *Biochemistry*, **34**, 7322–7334.
21. Kuipers, O. P., Kerver, J., van Meersbergen, J., Vis, R., Dijkman, R. M., Verheij, H. M. & de Haas, G. H. (1990). Influence of size and polarity of residue 31 in porcine pancreatic phospholipase $A_2$ on catalytic properties. *Protein Eng.* **3**, 599–603.
22. Yu, B.-Z., Poi, M. J., Ramagopal, U. A., Jain, R., Ramakumar, S., Berg, O. G. *et al.* (2000). Structural basis of the anionic interface preference and k∗cat activation of pancreatic phospholipase $A_2$. *Biochemistry*, **39**, 12312–12323.
23. Rajakannan, V., Yogavel, M., Poi, M.-J., Arockia Jeyaprakash, A., Jeyakanthan, J., Velmurugan, D. *et al.* (2002). Observation of additional calcium ion in the crystal structure of the triple mutant K56,120,121M of bovine pancreatic phospholipase $A_2$. *J. Mol. Biol.* **324**, 755–762.
24. Laskowski, R. A., MacArthur, M. W., Moss, D. S. & Thornton, J. M. (1993). PROCHECK: a program to check the stereochemical quality of protein structures. *J. Appl. Crystallog.* **26**, 283–291.
25. Ramachnadran, G. N. & Sasisekharan, V. (1968). Conformation of polypeptides and proteins. *Advan. Protein Chem.* **23**, 283–438.
26. Sekar, K., Sekharudu, C., Tsai, M.-D. & Sundaralingam, M. (1998). 1.72 Å resolution refinement of the trigonal form of bovine pancreatic phospholipase $A_2$. *Acta Crystallog. sect. D*, **54**, 342–346.
27. Sekar, K. & Sundaralingam, M. (1999). High-resolution refinement of orthorhombic bovine pancreatic phospholipase $A_2$. *Acta Crystallog. sect. D*, **55**, 46–50.
28. Verheij, H. M., Volwerk, J. J., Jansen, E. H., Puyk, W. C., Dijkstra, B. W., Drenth, J. & de Haas, G. H. (1980). Methylation of histidine-48 in pancreatic phospholipase $A_2$. Role of histidine and calcium ion in the catalytic mechanism. *Biochemistry*, **19**, 743–750.
29. Yuan, W. & Gelb, M. H. (1988). Phosphonate-containing phospholipid analogs as tight-binding inhibitors of phospholipase-$A_2$. *J. Am. Chem. Soc.* **110**, 2665–2666.
30. Renetseder, R., Brunie, S., Dijikstra, B. W., Drenth, J. & Sigler, P. B. (1985). A comparison of the crystal structures of phospholipase $A_2$ from bovine pancreas and *Crotalus atrox* venom. *J. Biol. Chem.* **260**, 11627–11634.
31. Kumar, A., Sekharudu, C., Ramakrishnan, B., Dupureur, C. M., Zhu, H., Tsai, M.-D. & Sundaralingam, M. (1994). Structure and function of the catalytic site mutant Asp 99 Asn of phospholipase A2: absence of the conserved structural water. *Protein Sci.* **3**, 2082–2088.
32. Sekar, K., Yu, B.-Z., Rogers, J., Lutton, J., Liu, X., Chen, X. *et al.* (1997). Phospholipase $A_2$ engineering. Structural and functional roles of the highly conserved active site residue aspartate-99. *Biochemistry*, **36**, 3101–3114.
33. Sekar, K., Biswas, R., Li, Y., M, D. & Sundaralingam, M. (1999). Structures of the catalytic site mutants D99A and H48Q and the calcium-loop mutant D49E of phospholipase $A_2$. *Acta Crystallog. sect. D*, **55**, 443–447.
34. Huang, B., Yu, B.-Z., Rogers, J., Byeon, I. J., Sekar, K.,

Chen, X. *et al.* (1996). Phospholipase $A_2$ engineering. Deletion of the C-terminus segment changes substrate specificity and uncouples calcium and substrate binding at the zwitterionic interface. *Biochemistry*, **36**, 12164–12174.
35. Kuipers, O. P., Dijkman, R. M., Pals, C. E., Verheij, H. M. & de Haas, G. H. (1989). Evidence for the involvement of tyrosine-69 in the control of stereospecificity of porcine pancreatic phospholipase $A_2$. *Protein Eng.* **2**, 467–471.
36. Steiner, R. A., Rozeboom, H. J., de Vries, A., Kalk, K. H., Murshudov, G. N., Wilson, K. S. & Dijkstra, B. W. (2001). X-ray structure of bovine pancreatic phospholipase $A_2$ at atomic resolution. *Acta Crystallog. sect. D*, **57**, 516–526.
37. Deng, T., Noel, J. P. & Tsai, M.-D. (1990). A novel expression vector for high-level synthesis and secretion of foreign proteins in *Escherichia coli*: overproduction of bovine pancreatic phospholipase $A_2$. *Gene*, **93**, 229–234.
38. Brunger, A. T. (1992). Free *R*-value: a novel statistical quantity for assessing the accuracy of crystal structures. *Nature*, **355**, 472–474.
39. Brunger, A. T., Adams, P. D., Clore, G. M., DeLano, W. L., Gros, P., Kunstleve, G. R. G. *et al.* (1998). Crystallography & NMR system: a new software suite for macromolecular structure determination. *Acta Crystallog. sect. D*, **54**, 905–921.
40. Otwinowski, Z. (1993). Oscillation data reduction program. In *Proceedings of the CCP4 Study Weekend: Data Collection and Processing, 29–30 January 1993* (Sawyer, L., Isaacs, N. & Bailey, S., eds), pp. 56–62, Daresbury Laboratory, Warrington, UK.
41. Otwinowski, Z. & Minor, W. (1997). Processing of X-ray diffraction data collected in oscillation mode. *Methods Enzymol.* **276**, 307–326.
42. Jones, T. A. (1985). Diffraction methods for biological macromolecules. Interactive computer graphics: FRODO. *Methods Enzymol.* **115**, 157–171.
43. Bernstein, F. C., Koetzle, T. F., Williams, G. J. B., Meyer, E. F., Jr, Brice, M. D., Rodgers, J. R. *et al.* (1977). The Protein Data Bank: a computer-based archival file for macromolecular structures. *J. Mol. Biol.* **112**, 535–542.
44. Kraulis, P. J. (1991). MOLSCRIPT: a program to produce both detailed and schematic plots of protein structures. *J. Appl. Crystallog.* **24**, 946–950.

***Edited by Sir A. Klug***

*(Received 10 June 2003; received in revised form 11 August 2003; accepted 15 August 2003)*